

Evolution of the chemical enrichment and the Mass-Metallicity relation in CALIFA galaxies

A. Camps-Fariña¹*, S. F. Sanchez¹, E. A. D. Lacerda¹, L. Carigi¹,
R. García-Benito², D. Mast^{3,4}, L. Galbany⁵

¹*Instituto de Astronomía, Universidad Nacional Autónoma de México, Apartado Postal 70-264, CP 04510 Ciudad de México, México*

²*Instituto de Astrofísica de Andalucía (CSIC), PO Box 3004, 18080 Granada, Spain*

³*Observatorio Astronómico de Córdoba, Laprida 854, X5000BGR, Córdoba, Argentina.*

⁴*Consejo de Investigaciones Científicas y Técnicas de la República Argentina, Avda. Rivadavia 1917, C1033AAJ, CABA, Argentina.*

⁵*Departamento de Física Teórica y del Cosmos, Universidad de Granada, E-18071 Granada, Spain.*

Submitted 2020 September 2

ABSTRACT

We use fossil record techniques on the CALIFA sample to study how galaxies in the local universe have evolved in terms of their chemical content. We show how the metallicity and the mass-metallicity relation (MZR) evolve through time for the galaxies in our sample and how this evolution varies when we divide them based on their mass, morphology and star-forming status. We also check the impact of measuring the metallicity at the centre or the outskirts. We find the expected results that the most massive galaxies got enriched faster, with the MZR getting steeper at higher redshifts. However, once we separate the galaxies into morphology bins this behaviour is not as clear, which suggests that morphology is a primary factor to determine how fast a galaxy gets enriched, with mass determining the amount of enrichment. We also find that star-forming galaxies appear to be converging in their chemical evolution, that is, the metallicity of star-forming galaxies of different mass is very similar at recent times compared to several Gyr ago.

Key words: galaxies: evolution – galaxies: abundances – galaxies: fundamental parameters

1 INTRODUCTION

The interstellar medium (ISM) and stars form a cycle in which the latter are born from the former. The ISM itself has been enriched with metals from the previous generations of stars. Finally, these new stars will in turn further enrich the ISM for the following generations of stars to be formed in, closing the duty-cycle. The metal content of the ISM at a particular time gets effectively "locked" in the chemical composition of the stars that were formed at that time.

As galaxies evolve, their metal content generally increases as a result of star formation, with other physical processes being capable of removing or diluting it, such as outflows and inflows (San-cisi, et al. 2008; Davé, Finlator & Oppenheimer 2011; Lilly, et al. 2013; Belfiore, et al. 2016; Barrera-Ballesteros, et al. 2018). These processes, as well as star formation itself, depend on the physical parameters of the galaxy such as the halo, stellar, and gas masses or the morphology and as a result the metal content of galaxies also correlates with them. Lequeux, et al. (1979) pioneered such studies showing that the total mass of a galaxy, inferred from the rotational velocity, correlates with the metallicity. Tremonti, et al. (2004) used 53,000 galaxies from the SDSS survey to show that the physical

parameter that gave the tightest correlation with the metallicity is the mass of the galaxy. Further explorations have confirmed that relation using non aperture biased spatially-resolved or integrated spectroscopic data (e.g. Rosales-Ortega, et al. 2012; Sánchez, et al. 2013; Zahid, et al. 2014; Lara-López, et al. 2013; Sánchez, et al. 2017).

The reason the mass-metallicity relation (MZR) is a fundamental relation for the evolution of galaxies is that its shape is directly related to the processes that regulate the star-formation in galaxies. At low masses the relation is nearly linear, which is expected of a closed-box model. At high masses, though, the MZR flattens towards an asymptotic value of the metallicity (Tremonti, et al. 2004). This value depends on the calibrator used (Kewley & Ellison 2008; Barrera-Ballesteros, et al. 2017; Sánchez, et al. 2017, 2019) as well as on the shape of the IMF which affects metal production with a steeper IMF producing less metals (Lian, Thomas & Maraston 2018).

The MZR is calculated based on global properties of galaxies, but this relation has an equivalent version within them: by comparing the surface mass to the local metallicity we obtain the resolved MZR or rMZR. This relation and how it compares to its global counterpart are an ongoing topic of research (Moran, et al. 2012; Rosales-Ortega, et al. 2012; Sánchez, et al. 2013; Erroz-Ferrer, et

* E-mail: acamps@astro.unam.mx

al. 2019), but in this article we are interested only in the properties of the global MZR.

The studies mentioned so far use the nebular metallicity rather than the metallicity of the stars. Nebular metallicity is measured from the properties of the emission lines produced by the ionised gas. The oxygen abundance is a well-established proxy for this quantity and it is much easier to measure compared to the metallicity in stars owing to the intense emission lines this element produces. In order to obtain the metallicity for the stars the stellar continuum needs to be fitted with stellar templates, using the former's shape and absorption lines to recover the properties of the stellar population which are weaker features on a spectrum.

On the other hand, the nebular metallicity can only be measured in gas-rich, star-forming galaxies and it only gives us information regarding the current values of the metallicity in a galaxy. The evolution of the gas metallicity can be probed by observing galaxies at increasing redshift. Studies have generally found that galaxies have a growth in metallicity (e.g. Steidel, et al. 2014; Troncoso, et al. 2014; Wuyts, et al. 2014; Sanders, et al. 2015; Onodera, et al. 2015; Kashino, et al. 2017; Cullen, et al. 2019). The speed of this change depends on mass in agreement with the observed phenomenon of downsizing which shows that the more massive galaxies appear to have evolved faster in all aspects, assembling their masses earlier and in this case getting enriched faster too.

Stellar metallicity is explored using a completely different technique: the fossil record method. This technique allows us to fit templates associated with stellar populations of a particular age and metallicity (or having a particular star-formation history, e.g., Bitsakis, et al. 2018) to the observed stellar spectra or particular features in that spectra, like the stellar indices (Kauffmann, et al. 2003). We can use the recovered weights for each population to analyse the current stellar composition of the galaxy or, as is the goal of this article, to estimate the evolution of the metallicity and the mass-metallicity relation in galaxies. A particularly noteworthy advantage of this type of analysis is that we can measure the evolution of the same sample of galaxies through time, rather than observing different galaxies at different times as is the case for high-redshift observations.

Pioneering work on this topic was done by Panter, et al. (2008), who determined the MZR of SDSS galaxies at different redshifts using simple stellar population (SSP) fitting and then compared these results to the ones from Tremonti, et al. (2004) and similar works which measured gas metallicities. Vale Asari, et al. (2009) measured stellar metallicities of SDSS galaxies derived from fitting SSP templates with *STARLIGHT* to show the evolution of the MZR slope in time. However, they focused on the more massive galaxies for which the nebular metallicity cannot generally be obtained. Previously, Gallazzi, et al. (2005) proved that the stellar MZR presents a shape similar to the one reported for the nebular MZR. This shape seems to be preserved in the spatially resolved MZR with both of them showing a clear evolution with an enrichment of massive galaxies (González Delgado, et al. 2014)

In this article we use the CALIFA dataset of Integral Field Spectroscopy (IFS) observations of galaxies in the nearby universe to measure the metallicity and mass-metallicity relation at different times throughout the galaxies' lifetime. We also separate the galaxies depending on their masses (for the evolution of the metallicity), morphology and star forming status and analysed the impact of these on the results. The metallicities were measured at the effective radius, but we also check how the results change depending on galactocentric distance.

The article is organised as follows: in Section 2 we describe

the sample of galaxies that we use and their data; in Section 3 we describe the analysis of the data with a summary of the products of the reduction and analysis pipeline for the survey, including a description of how the quantities were calculated and the method to average the quantities in a consistent manner; in Section 4 we present the results of the analysis, showing the evolution of the metallicity and the mass-metallicity relation, as well as a proxy for the star-formation. We also show how the evolution of these parameters is affected by the galaxies' morphology and star-forming status, as well as the galactocentric distance at which it is measured; finally, in Section 5 we discuss the validity of our results and the impact and relevance that they have on our understanding of the evolution of galaxies.

2 SAMPLE AND DATA

The base sample we used consists of all galaxies from the CALIFA survey with good spectroscopic data up to DR3 using the low-resolution setup (V500). In addition, we included objects observed by CALIFA extended surveys (Sánchez, et al. 2016), including those of the PMAS/Ppak Integral-field Supernova hosts Compilation (PISCO; Galbany et al. 2018). This results in an initial sample of 877 galaxies. This sample follows the criteria of the CALIFA mother sample (MS; Walcher, et al. 2014) in a way that all objects have their optical extension inside the FoV of the instrument, but some could be slightly fainter or brighter than those in the original MS. Moreover, some objects have their redshifts slightly above the boundary of the CALIFA original selection (with this extended sample z goes up to 0.08, but with 93 per cent of them below 0.035). We further refined the sample by removing those galaxies which are known to host an AGN (Lacerda, et al. 2020) as well as those with an inclination above 70° or which appear to be interacting. After this selection we ended with the final sample of 529 galaxies which we use in this article, comprising a stellar-mass range of $10^{7.8} - 10^{12.2} M_\odot$ with the mean value of $10^{10.4} M_\odot$.

The CALIFA V500 setup adopted along this study covers a wavelength range between 3745\AA and 7200\AA , providing with a spectral resolution of $\text{FWHM} \sim 6.5\text{\AA}$, through all the considered spectral range. The PPAK fibre bundle (Kelz, et al. 2006) provides with a central bundle of 331 fibers of $2.7''$ /diameter fibres, that cover an hexagonal field-of-view of $74'' \times 64''$ with a filling factor of slightly less than a 60% (an additional set of 36 fibres are distributed in 6 mini-bundles far away from this central one to sample the night-sky). In order to obtain a 100% coverage of the FoV, also increasing slightly the spatial resolution, a three-pointing dithering scheme was adopted along all the observations considered here (Sánchez, et al. 2012). Thus, after a standard reduction procedure (Sánchez 2006) the final product is a data-cube with two dimensions corresponding to the spatial coordinates and the third one sampling the wavelength range. The reduction comprises spectral extraction, wavelength calibration, sky subtraction, fibre transmission correction, flux calibration, cube reconstruction, differential atmospheric correction, and image registration. The variance was propagated along the different reduction steps and stored in an additional data-cubes, together with a mask of the bad pixels (including cosmic rays and vignetting), and a map of the variance covariance due to the different reduction steps. The final data-cubes have a spatial resolution of $\text{FWHM} \sim 2.5''$ and a sampling of $1''$, and a photometric accuracy better than a 5% through all the considered wavelength range. For further details on the data, the reduction and the quality, we refer

the reader to [Husemann, et al. \(2013\)](#); [García-Benito, et al. \(2015\)](#); [Sánchez, et al. \(2016\)](#).

The morphological classification for the galaxies from the DR3 sample is obtained from [Walcher, et al. \(2014\)](#). The classification of the remaining galaxies is conducted using the same scheme employed by [Walcher, et al. \(2014\)](#). The procedure involves a by-eye inspection of the true-colour SDSS (DR7; [Abazajian, et al. 2009](#)) images. For those galaxies that are not present in this set of images, we use (i) similar images extracted from the CALIFA datacubes, which have lower spatial resolution, and (ii) emission-lines maps (described later on), in order to trace possible spiral arms structures. At the end, the morphological distribution is: 131 ellipticals (E0-E7), 73 lenticulars (S0+S0a), 325 spirals (Sa-Sm) and irregular (I) galaxies. This classification scheme was adopted previously in [Lacerda, et al. \(2020\)](#) and [Espinosa-Ponce, et al. \(2020\)](#) for the same sample of galaxies.

3 ANALYSIS

3.1 Pipe3D

The stellar population synthesis of all datacubes is performed by *Pipe3D* ([Sánchez, et al. 2016,?](#)), adopting the GSD156 library of SSP ([Cid Fernandes, et al. 2013](#)). The GSD base is a combination of the SSP spectra provided by [Vazdekis et al. \(2010\)](#) for populations older than 63 Myr and the [González Delgado et al. \(2005\)](#) models for younger ages. This SSP-library includes 156 different templates comprising 39 stellar ages (from 0.001 to 14.1 Gyr, with uneven steps) and four metallicities (0.2, 0.4, 1 and 1.5 Z/Z_{\odot}) using the initial mass function (IMF) by ([Salpeter 1955](#)). A wide set of previous studies used this same library ([Pérez, et al. 2013](#); [González Delgado, et al. 2014](#); [Cano-Díaz, et al. 2016](#); [Sánchez-Menguiano, et al. 2016](#); [Ibarra-Medel, et al. 2016](#); [Sánchez, et al. 2018](#); [Lacerda, et al. 2020](#)), where one can find more details and caveats about the fitting procedure.

The basic result of the stellar population analysis performed by *Pipe3D* is the fraction of light in a certain wavelength (the V-band in our case) that each SSP contributes to the observed spectrum. This fraction of light (or weight) can be transformed to luminosity (considering the monochromatic luminosity at the considered fraction), and finally to a stellar mass (M_*) via the Mass-to-Light ratio of each SSP. Thus, the analysis provides with the amount of mass (and light) corresponding to stars of a certain age and metallicity. The first moment of this distribution along the ages and metallicities are the so-called Mass- (Luminosity-) weighted age and metallicity (LW and MW, respectively, e.g., [Sánchez, et al. 2016](#)). These mean values are frequently used to characterise the stellar population, despite the fact that they are very rough estimation of the real distribution of ages (and metallicities).

By correcting the described mass distributions by the M_* reduction as a result of star deaths that would have occurred from a particular time to the present (i.e., the look-back time corresponding to the age of the stars corrected by the redshift of the galaxy) it is possible to derive the amount of M_* formed at any previous time (discretized by the age sampling of the SSP). The corresponding cumulative function from the beginning of the Universe to the current time is known as the Mass-Assembly History (MAH). The MAH, and its derivative along the time (the Star-formation History, SFH) has been extensively used to determine which galaxies (and regions of galaxies) form before and at which speed, being the key evidence of both the galaxy downsizing: massive galaxies ensemble

their mass earlier and faster than less massive ones ([Thomas, et al. 2005, 2010](#); [Pérez-González, et al. 2008](#)). It has been used too to demonstrate the so-called local/resolved downsizing ([Pérez, et al. 2013](#); [Ibarra-Medel, et al. 2016](#); [García-Benito, et al. 2017](#)): more massive regions in galaxies (ie., the center) are formed before and faster than less massive regions (i.e. the outer areas).

The fraction of light provided by this analysis can be used to derive not only the stellar-mass distribution along the time, but also a similar distribution for the stellar metallicity. In this case, at any look-back time, it is possible to derive the LW- (and MW-) metallicity of the stars formed before that time. They are estimated as the first moment of the metallicity distribution for all ages older than the considered look-back time (LBT), correcting the fractions by the mass-loss from their formation to the observing time (i.e., the considered LBT). Estimated along the full Hubble time they correspond to the LW and MW- stellar metallicities described before. The metallicity distribution along the LBT comprises the chemical enrichment history (ChEH) of a galaxy (or a region of a galaxy).

We should note here that this derivation is based on the assumption that the decomposition of the stellar population in the adopted SSP is accurate, precise, and unique. The reality is far from this assumption. Different authors have already explored the many degeneracies inherent to the adopted analysis. We point the reader to [Walcher, et al. \(2011\)](#); [Sánchez-Blázquez, et al. \(2011\)](#) to understand the limitations of the adopted methodology. Along this study we have intentionally ignored those limitations, describing the current results based on a single adopted methodology, a particular SSP library, and a considered dataset.

3.2 Averaging of properties

In order to obtain average properties of a group of galaxies we need to make sure that the measurements are made in consistent physical scales so that the results are directly comparable. This allows us to stack the properties and perform averages for each grouping. For the spatial scale we use the effective radius (R_e ; defined as the radius which contains half the light emitted by the galaxy) as a scaling quantity to average the properties of galaxies of different sizes. The metallicities for each galaxy are calculated at R_e , which is a good indicator of the global metallicity of a galaxy ([Sánchez, et al. 2017](#)). Many other physical quantities measured at the R_e seems to be a good proxy of the average properties of galaxies ([González Delgado, et al. 2015](#); [Sánchez 2020](#)). *Pipe3D* also provides the values for the slope of the metallicity gradient, which will allow us to check the effects of measuring the metallicity at R_e instead of at the centre or the outskirts (defined here as twice the R_e).

The temporal scale of the data, on the other hand, needs to be corrected. While all the galaxies in the sample are located within the nearby universe they still have different redshifts. This means that we are effectively observing each galaxy at a slightly different cosmic time due to a difference in how long it took the light we are observing now to arrive. This effect is accounted for in our data by correcting the age of the fitted stellar templates with the redshift. The individual ChEHs, then, are shifted from one another in time. This affects the edges of the timeline the most: the more recent and more remote LBT in the timeline are not populated by all galaxies. Thus, we re-sample the individual time-evolution tracks of the metallicity to a common single timeline corresponding to the median of the individual time-lines for each averaged ground. A similar correction (and effect) was described in the analysis of the Mass-Assembly histories described by [Ibarra-Medel, et al. \(2016\)](#). However, in their case the effect is stronger due to a much wider range in redshift of the

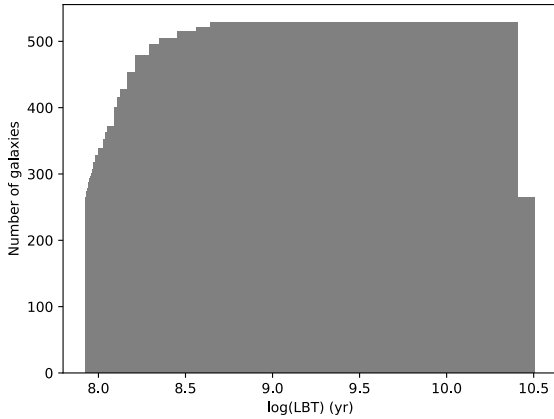


Figure 1. Histogram of the coverage of the median time-line, showing the number of galaxies that populate each time.

bulk population of analysed galaxies (extracted from the MaNGA survey, [Bundy, et al. 2015](#), that reaches up to $z \sim 0.17$).

Once we have determined the representative timeline we re-sample each of the ChEHs via linear interpolation, discarding those values that lie out of range. This method does not guarantee that all the LBT points contain all the galaxies in the sample, as indicated before. If we wanted to ensure this we would have needed to choose the time-line as only the overlap between all galaxies in the sample, discarding data points corresponding to LBT values which are covered by a sufficient number of galaxies to be statistically significant but which do not contain all of them. We chose the median time-line as a good compromise to get a good range of LBT and avoid a lack of statistical significance at the edges.

In Fig. 1 we show the number of galaxies that populate each time. Above ~ 400 Myr ($10^{8.6}$ yr) all galaxies are represented except in the very last value for the time. The minimum number of galaxies is 265, which occurs at both edges.

After interpolating all the ChEHs into the same timeline we can proceed to average them. We group the galaxies into mass, morphology and star-forming status bins (or any combination of these) in order to see how these parameters affect the ChEHs.

The averaging is conducted in two steps. First, we calculate the mean value of the ChEH for each galaxy over the temporal range where all galaxies within a particular group have measured values of the metallicity. We take the average of these values and then shift all ChEHs by the difference, which in general terms bundles the ChEHs together. After this we perform the average of the shifted ChEHs. The reason we perform this is to prevent outliers from affecting the sample too much. As an example, consider the case where one galaxy in a group has a very low metallicity and its high redshift meant its individual ChEH was not sampled for much of the recent time-line. In this case if we performed the average normally the galaxy would noticeably affect the metallicity only for a portion of the timeline, artificially creating what would appear to be an growth in metallicity for the group in question. By shifting them beforehand the effect of any outlier is applied to the averaged ChEH over the whole timeline instead, preventing the appearance of such artefacts.

Performing the averaging in this manner has an additional advantage: we can separate the variance of the ChEHs within a group of galaxies into two types: The variance due to the separation

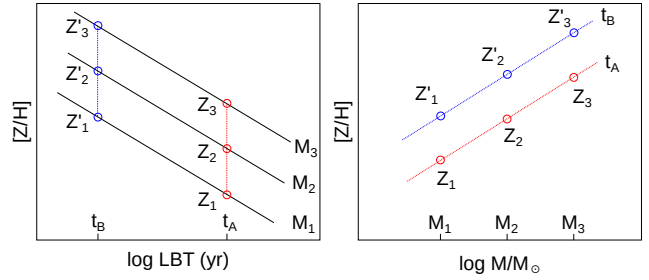


Figure 2. Illustration of the process to obtain the MZR from the ChEHs. By sampling the three ChEHs (for three mass bins) vertically we select specific times and obtain the metallicities at different masses, immediately producing the MZR at two different times.

between individual ChEHs and the variance due to the different shapes of the ChEHs. This constitutes an additional result which allows us to infer whether galaxies in a group have similar evolutions and whether they have a wide range of terminal metallicity values.

We also want to obtain the evolution of the MZR, which we derived from the ChEHs. Only this time we used different mass bins in order to properly sample the MZR. Then we can invert the relation between metallicity, LBT, and mass by making "vertical cuts" on the ChEHs. Thus, we select different times and obtain the metallicity for each mass bin. This immediately produces the mass-metallicity relation graphs at different times.

In Fig. 2 we show an illustration of the process, where three ChEHs for three mass bins are used to obtain the MZR at two different times.

The mass bins used for this calculation are defined as being 0.5 dex wide with a 0.25 dex step. This means that half of each bin overlaps with the previous bin and half with the next one. This allows for a smoother transition between mass values.

The last parameter studied in this article is the mass variation, which we use as a proxy for the star formation rate (SFR). It is obtained from the changes in mass divided by the time step (essentially dM_*/dt). The mass variation has two contributions, the increase in mass due to star formation and the decrease due to dying stars. The latter is a minor, steady decrease that does not contribute much to the mass variation ($\sim 5\%$) which justifies our use of the mass variation as a proxy for the SFR. We indicate this quantity as SFR' in the article.

The uneven sampling of the LBT means that at recent times the time-steps are smaller and therefore the SFR' is more affected by the errors in the determination of the M_* and SSP age, a result of dividing small increments in mass over small increments in time. In order to minimise this effect we fit a non-smoothing spline to the cumulative mass function and then take its numeric derivative as the mass variation. This mitigates the effect of the errors associated with the resolution.

In Fig. 3 we show the mass evolution and SFR' for three galaxies. It can be seen that at recent times the SFR' oscillates, a result of the aforementioned small increments in time and mass. In order to average SFR' within a particular bin we calculate the individual SFR' curves in the same manner as we did for the ChEHs and then proceed similarly, first re-sampling them into a single timeline and then averaging them within the defined bins. The evolution of the SFR' shown here is compatible with the results for the evolution of the SFR depending on mass shown in previous studies ([Panter et al. 2007](#); [López Fernández et al. 2018](#); [Sánchez, et al. 2019](#)), which

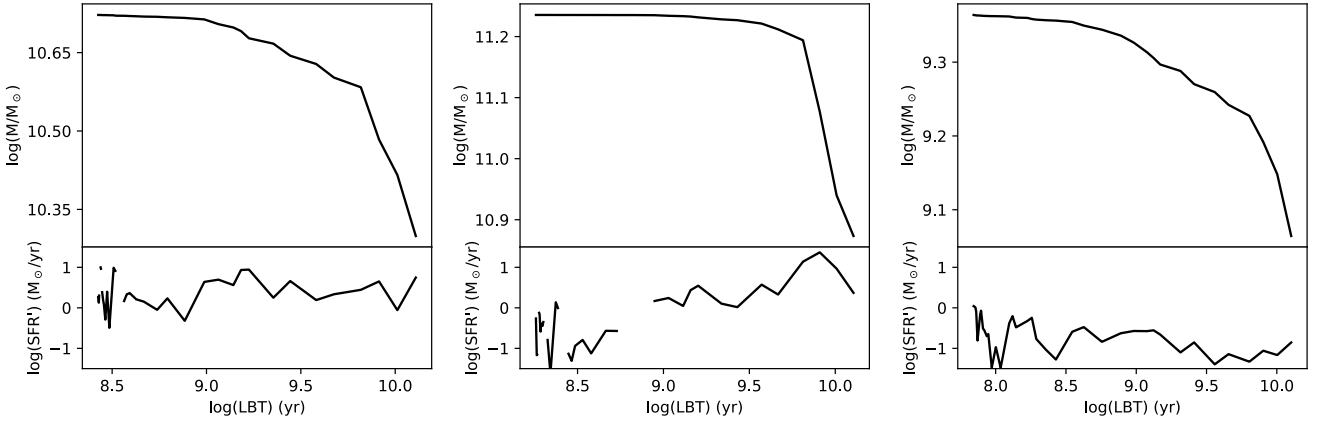


Figure 3. Three examples of the mass evolution (above) and the resulting mass variation (below). At recent times the divergence of the mass variation is clearly observed. The gaps in the lines correspond to values of 0, which diverge upon taking the logarithm.

show how the more massive galaxies evolved faster with high SFR at early times that have declined, while the less massive galaxies show flatter profiles.

4 RESULTS

In this section we present the results for the evolution of the metallicity and the MZR, obtained from the fitting of stellar populations described above. The metallicity we present here is a weighted average of the metallicities within an LBT bin over the galaxy and measured at the effective radius. One can weigh the metallicity of the populations via either their luminosity or their mass. All the following results correspond to the metallicity weighted by luminosity.

4.1 Evolution of the metallicity

In Fig. 4 we show the average metallicity as well as the SFR' as a function of time for all the galaxies in our sample, with the error of the mean shown as shaded areas. The most obvious feature is that the more massive galaxies are always more metallic than their lower mass counterparts. We can also observe that the more massive galaxies achieved their maximum metallicity (which in this case coincides with the current one) much earlier with the lowest masses still showing growth in metallicity. An apparent "dip" in metallicity is also observed between about $\sim 1\text{-}2.5$ Gyr ($10^9 - 10^{9.5}$ yr) in LBT. This dip is more prominent for the lower mass bins while not being visible for the highest mass ones. It could also be interpreted as a steep increase of the metallicity between two fairly flat chemical enrichment regimes.

The flatness of the profile for the more massive bins implies that for this population of galaxies the metallicity has reached its maximum value and they are no longer evolving from a chemical point of view. This lack of evolution can be partly explained as a result of the cumulative mass history of each galaxy, where each subsequent star-formation burst represents a lower percentage of the total mass of the galaxy being added. The relatively lower mass change then corresponds to a lower change in the global metallicity. Other than this, retired galaxies with no star formation will also not exhibit changes to their stellar metallicity regardless of the fact that their stars should still be enriching the ISM.

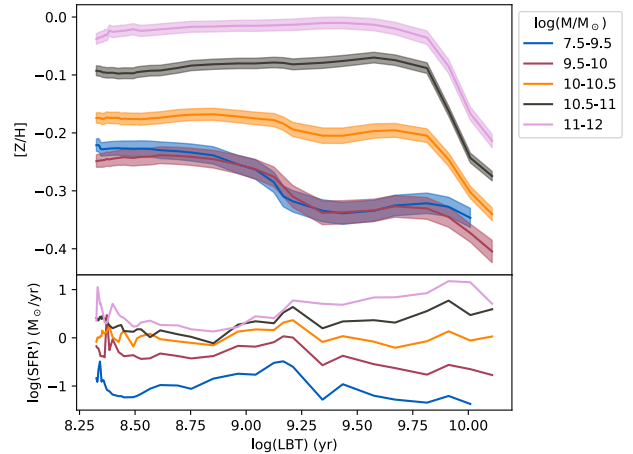


Figure 4. On top, the evolution of the metallicity as a function of the look-back time (LBT) for all the galaxies in the sample. Each line corresponds to a mass bin within which all the individual galaxies were averaged. The shaded areas represent the error of the mean ($\epsilon = \sigma/\sqrt{N}$), spanning the range between $Z/H - \epsilon_{Z/H}$ and $Z/H + \epsilon_{Z/H}$. The bottom panel shows the SFR' for the same bins.

The fact that the lowest mass bins exhibit a steady growth up to current times implies that these galaxies are still assembling their mass and therefore are continuing to form stars within their increasingly enriched ISM. We could interpret this as low-mass galaxies having a slower evolution, whereupon the growth in metallicity observed here corresponds to a much shorter time-step for the more massive galaxies. In this scenario, if we were to continue observations for several Gyr more the metallicity of these galaxies would eventually taper off. Thus, producing a curve similar to that of the more massive galaxies but stretched in the temporal axis.

The dispersion is reflected by the error of the mean, an indication that while we can describe average trends the individual galaxies have much more complicated SFHs and ChEHs and therefore the averages are just a first order trend that has to be strongly modulated by the individual processes in galaxies. It is clear, however, that the error of the mean is smaller in more massive galaxies

than for less massive ones. This implies that they have either more similar SFHs and ChEHs or that their differences appear at earlier times where we have less resolution. This is in agreement with the results by [Ibarra-Medel, et al. \(2016\)](#).

The SFR' curves show a clear negative evolution for the most massive bins, with a flatter, if bumpy, profile for the lower mass bins. The more massive galaxies also show higher values of the SFR' over time. The colours for the SFR' are equivalent to those of the ChEH, that is, a ChEH and a SFR' curve with the same colour within the same plot have been calculated using the same galaxies.

The most interesting feature of the SFR' curves, however, is the "bump" in star formation that we find between 1-3 Gyr ($10^9 - 10^{9.5}$ yr) in the LBT. This coincides perfectly with the "dip" that we detected in the ChEHs, and indeed they behave much in the same way, becoming more prominent for less massive galaxies.

4.1.1 Effect of morphology

In order to further evaluate how the properties of a galaxy affect its chemical enrichment we can separate the sample into morphology bins as described in section 2. Besides the final M_* , which has a clear influence on the SFHs in galaxies ([Pérez-González, et al. 2008](#); [Thomas, et al. 2010](#); [Pérez, et al. 2013](#); [González Delgado, et al. 2014](#); [Ibarra-Medel, et al. 2016](#)), it is known that morphology strongly affects (or it is affected by) how galaxies evolve ([Blanton & Moustakas 2009](#); [García-Benito, et al. 2017](#); [Sánchez 2020](#) and references therein). In general the morphology modulates the differences in evolution observed by mass.

In Fig. 5 we show the evolution of the stellar metallicity as well as the SFR' for the galaxies in our sample separated by morphology bins for different mass ranges. Within each box we also show in dotted lines the ChEHs for the entire sample (also shown at the top-left panel) for easy comparison. This allows us to quickly assess how the chemical evolution of a particular type of galaxies changes with respect to the full sample. Showing the errors of each bin as we did in Fig. 4 would not allow us to compare the ChEHs for each morphological bin with the full sample as the figures would be too loaded, so we indicate the typical error of the mean in bars on the lower left corner.

Early-type galaxies (E/S0) have consistently the highest metallicity values. This is especially true for the more massive bins which are more representative of the sample for these morphologies and have a higher number of objects, as can be seen from their lower error bars. This effect is also readily visible for spirals, with a clear trend from Sa to Sd galaxies of decreasing the metallicity, as well as a narrowing of the differences between different masses. Massive spirals also appear to exhibit a slight decrease in metallicity after the initial enrichment. However, it is fairly small compared to the uncertainties and therefore might not be statistically significant.

The earliest galaxy types also have substantially flatter profiles after the initial enrichment when compared to the later ones, which have increasingly steeper curves, especially for the Sc and Sd morphological bins. If we compare the low-mass bins for these morphological types with those for Sa and Sb (even for those in the E/S0 group) we can see that the ChEHs get progressively less flat, switching from a flat evolution to a positive increase. This effect can also be seen for the entire sample, but Sd galaxies show a much more pronounced increase in the lower mass bins compared to the entire sample or any other morphological type.

Another feature that appears to be affected by the separation into morphology types is the aforementioned "dip" in the ChEH. As was mentioned for Fig. 4 the dip gets deeper for lower mass

bins. However, here we also see that it gets more prominent within a mass bin for the latest morphological types. Whereas in Sa it can only be slightly detected for the lower mass bins it gets deeper as we progress to Sb, Sc, and finally Sd, where it is very prominent.

This feature correlates with the SFR' of the galaxies as was observed in Fig. 4. The latter morphology bins show clearer bumps in SFR' compared to their earlier counterparts. The correlation is less clear in morphology than it is in mass, for example Sa galaxies show clear bumps in SFR' even though the dip in $[Z/H]$ is barely visible only for the lowest mass bin. However, the general trend of both features being more prominent for latter and less massive galaxies can still be observed.

The results appear to suggest that at around redshift 0.1-0.2 (1-2.5 Gyr ago) there was a general episode of star formation which affected the metallicity of galaxies in the local universe. This would not necessarily mean that all galaxies hosted an increase in star formation because even if only a portion of the galaxies (especially low mass and late-type ones) had bursts of star formation, as long as these were powerful enough to affect the average then the same effect would be observed.

We should note here that this general episode of star-formation at the considered redshift has not been reported in the observed cosmological galaxy surveys (to our knowledge). However, this means little, since our procedure is recovering the SFH and ChEHs of individual galaxies, not of a population. For instance, a morphological or mass change from the current time to the event time may dilute this signal in a cosmological survey. On the other hand, if it was an artefact of the procedure, it is difficult to justify why it shows such a clear morphology/mass pattern.

4.1.2 Effect of star-forming status

Another parameter that can affect the chemical evolution of galaxies is whether or not they are still forming stars. Star-forming galaxies (SFG) have either sustained star formation (SF) throughout their life-times or they have experienced a massive recent burst of SF that rejuvenated them. Recent results, however, support better the first scenario ([Pandya, et al. 2017](#); [Sánchez, et al. 2019](#)) showing that galaxies currently in the star-forming main sequence have mostly stayed in that regime or oscillated in and out repeatedly through time.

This means that we would expect these galaxies to still be evolving in terms of their metallicity. Retired galaxies (RG) have stopped forming of new stars at the current observing time and therefore have an aged stellar population with no further evolution on their stellar metallicity. The current population of stars in retired galaxies continues to enrich the ISM, but without a new stellar population formed from this enriched gas, the stellar metallicity remains unchanged. Furthermore, it is not clear when these galaxies stopped their SF activity (and the subsequent stellar metal enrichment). Some recent studies support the idea that a substantial portion of those galaxies were SF \sim 1-4 Gyr ago ([Muzzin, et al. 2013](#); [Rodríguez-Puebla, et al. 2017](#); [Sánchez, et al. 2019](#)).

In Fig. 6 we show the evolution of the metallicity for galaxies in our sample separated by their current star-forming status. We defined the SFG group as galaxies with an average $EW_{H\alpha}$ over 10 \AA while RGs were defined as those with $EW_{H\alpha}$ below 3 \AA , leaving the Green Valley galaxies (GVG) as those within the two aforementioned values. These values were chosen to be consistent with the sample selections of [Lacerda, et al. \(2020\)](#). [Cano-Díaz, et al. \(2019\)](#) show that 5-6 \AA is a good value to separate a sample into SFG-RG groups as shown from the object density plots in the

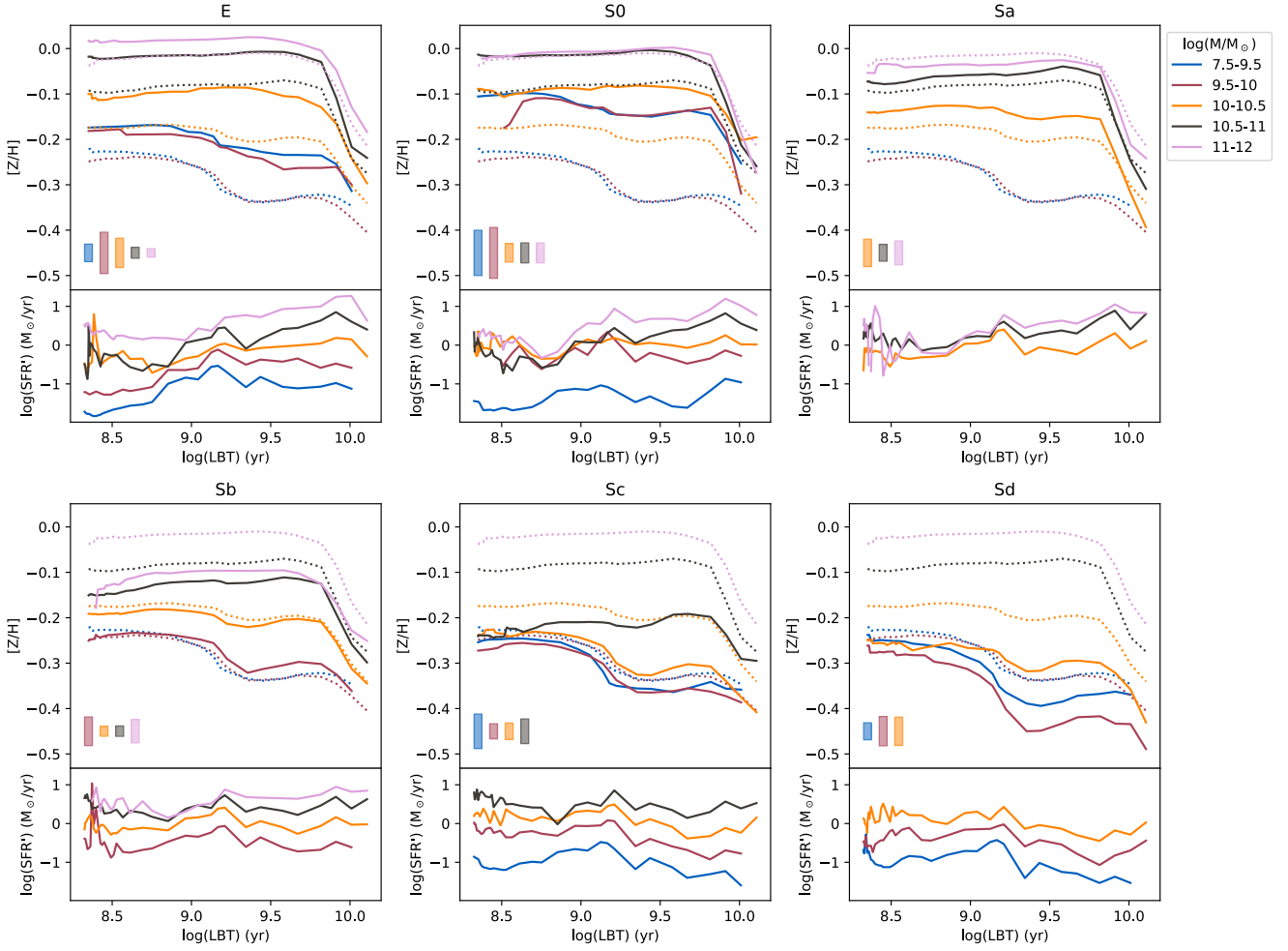


Figure 5. On the top box of each panel we show the evolution of the metallicity as a function of the LBT for each morphological bin of the galaxies in our sample. Each line corresponds to a mass bin for galaxies of the corresponding morphology. The galaxies within each bin were averaged to produce each individual ChEH. The dotted lines represent the ChEHs for all galaxies (as in Fig. 4). On the lower left corner of the top box in each panel the shaded areas represent the typical error of the mean for each ChEH. The bottom box of each panel shows the SFR* for the corresponding bins, in the same colours.

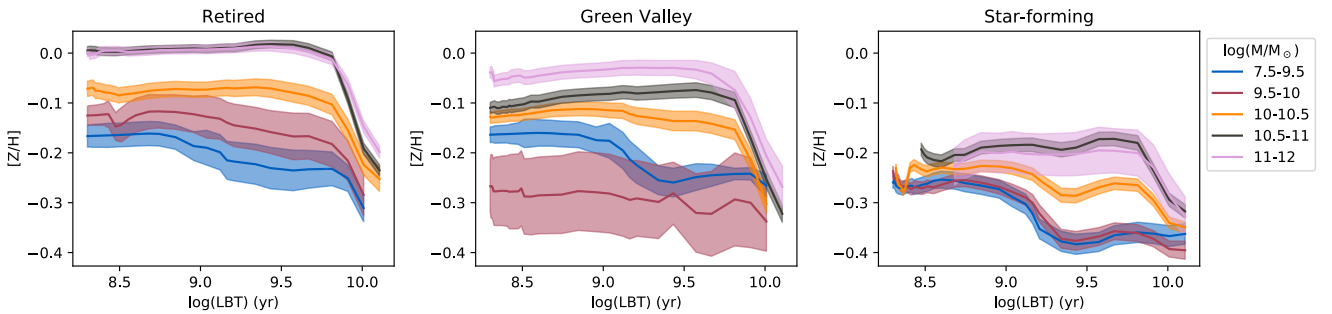


Figure 6. Evolution of the metallicity as a function of the look-back time (LBT) for all the galaxies in our sample, separated by their star-formation status. On the left-panel we show the retired galaxies, in the middle one those in the Green Valley, and finally on the right-panel the star-forming galaxies. Each line corresponds to a mass bin within which all the individual galaxies within the corresponding star-forming status were averaged. The shaded areas represent the error of the mean for each ChEH.

Table 1. Distribution of galaxies in the sample regarding their star-forming status

	RG	GVG	SFG
Total	218	81	230
E	122	7	2
S0	63	4	6
Sa	21	23	9
Sb	9	42	88
Sc	1	3	69
Sd	2	2	56

Notes. Table showing the number of galaxies in each star-forming status in total and divided by morphology.

SFR- M_* diagram. The values we use allow us to define the GVG group of galaxies while also ensuring that the objects contained in the SFG and RG groups are robust identifications.

In Table 1 we show the number of galaxies in each star-forming status group, with further detail as to the morphological makeup of each group.

It is important to mention that the SFG-GVG-RG separation is not independent from the separation by morphology. SFG are predominantly late-type galaxies while RG are mostly early type E and S0 galaxies (e.g. Young, et al. 1996; Sánchez, et al. 2007; Cano-Díaz, et al. 2019) which can be clearly be observed in Table 1. As such, the main results observed from separating the galaxies by morphology still apply: RG have higher metallicity values and were enriched faster than their SFG counterparts, with GVG in between both of them. GVG, however, appear to be closer to RG in their chemical evolution than to SFG.

An interesting new feature can be observed in the SFG group, in that the current metallicities for all mass bins appear to somewhat converge. This is opposite to what we observe for GVG and RG which maintain a gap between the metallicity of their mass bins. SFG do appear to have a wide gap between bins initially, but it then steadily narrows.

This suggests that some form of regulatory process occurs in SFG which limits the maximum value the metallicity can reach, thus as galaxies evolve they converge around that value. The two most massive bins have mostly flat curves with a metallicity value substantially lower than that of the other groups, while the lower mass bins have increased their metallicity steadily but are now flattening around the same value.

As mentioned above, low mass galaxies tend to be still getting enriched in metallicity, which is observed here mostly for SFG with a steep growth, but it is also observed in GVG and RG albeit in a much more subdued manner. This phenomenon is similar to what is observed comparing the early to late type galaxies, so it is likely to be a result of morphology.

RG show a clear progression in M_* with all the ChEHs having a similar shape but with an initial enrichment that ends earlier with increasing mass. This is a clear result of downsizing, with the more massive galaxies assembling their mass faster.

4.2 Evolution of the mass-metallicity relation

In the previous section we analysed how the values of the stellar metallicity have evolved in cosmic time for the galaxies in our sample. In this section we will perform a similar analysis for the MZR. We can use the parameters obtained from our analysis to explore how this relation has changed throughout time for the galaxies in our sample.

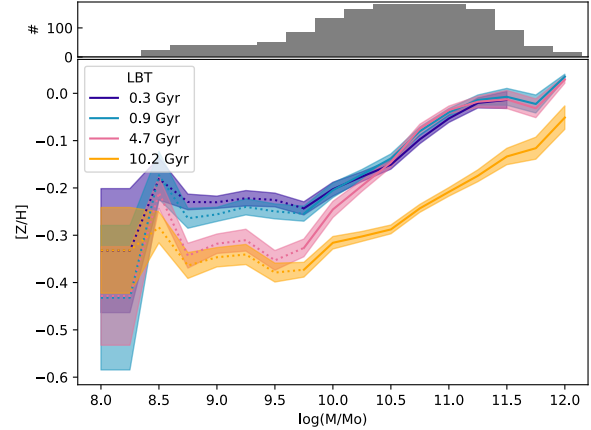


Figure 7. Evolution of the mass-metallicity relation (MZR) in time for all the galaxies in the sample. Each line represents the MZR at a particular look-back time (LBT) as indicated by the colour. The shaded areas represent the error of the mean ($\epsilon = \sigma/\sqrt{N}$), spanning the range between $Z/H - \epsilon_{Z/H}$ and $Z/H + \epsilon_{Z/H}$. On the top panel we show the distribution of galaxies along the mass range.

It is expected that galaxies with higher mass both achieve higher values of the metallicity and evolve faster, a fact that could already be observed to an extent in the previous section. On the contrary, galaxies in the lower mass bins appeared to still be in the process of increasing their metallicity.

A faster evolution of higher mass galaxies should manifest in the MZR as a change in slope over time, with the relation being steeper in earlier times as the more massive galaxies should have already been enriched while the less massive galaxies would be much slower. Then, as time passes, the relation gets shallower as the lower mass area increases its metallicity while the high mass galaxies maintain the values from earlier times.

In Fig. 7 we show the MZR for several values of the LBT for the galaxies in our sample. The expected change in slope is clearly observed: the higher mass galaxies quickly get enriched, which initially makes the slope steeper. On the contrary, the lower mass galaxies get enriched much slower, steadily making the slope shallower once more, but at higher overall values of the metallicity.

The lowest LBT bin in the figure does not cover the highest values in the considered mass range. This is a result of the fact that the few most massive galaxies in our sample are not in our immediate vicinity, so as a result of having a higher redshifts their lowest LBT value is higher than the lowest LBT bin. In other words, there is no overlap between very high mass and very low redshift values for the galaxies in our sample. This is the result of an unavoidable selection effect: the higher mass galaxies also have a larger size, so if they were placed close to us they would not fit within the field of view of the instrument (e.g., Andromeda). Thus, this is a direct effect of the diameter selection of the sample, aimed to fit its optical extension with the FoV of the instrument. However, other selections, like the one proposed for the MaNGA survey with a wider range of redshifts (Bundy, et al. 2015; Wake, et al. 2017), do indeed produce an even stronger M_* -redshift effect, as highlighted by Ibarra-Medel, et al. (2016).

The MZR for those mass regions outside the range in which the CALIFA galaxies is considered to be complete (Walcher, et al. 2014) are represented with dotted lines. For the regimes whose

completeness we cannot guarantee the number of sampled galaxies is relatively low (Fig. 7, top panel). The combination of both effects preclude us to make strong conclusions on this regime. In particular, the results for the range of low-mass/dwarf galaxies should be taken with particular care.

Consistently with the previous caveat, it is observed that the mass range below about $10^{8.7}$ solar masses has very high fluctuations in the value for the metallicity, with similarly high errors. This is a consequence of the low amount of galaxies in our sample in this range with only a few objects.

4.2.1 Effect of morphology

As we did for the evolution of the metallicity we can divide our sample into morphology bins and calculate how the MZR evolves within each of them. Owing to the aforementioned caveat of a very low amount of galaxies below $10^{8.7}$ solar masses, which already made results for the full sample in this range unreliable, the MZR below this value was removed in the morphology bins. We also removed any mass-metallicity data point that did not have at least 3 galaxies contributing to it.

In Fig. 8 we show the MZR calculated for each morphological bin. The first thing that can be observed is that not all the boxes have the same coverage in mass. Indeed, this is a result of the fact that the earlier types of galaxy tend to be more massive than the later types. The extremes of this can be appreciated by comparing S0 to Sd, which have a very small overlap in their mass range.

A remarkable result that can be observed as we divide the sample into morphology bins is that most of the groups do not exhibit a change in the slope of the MZR after the initial enrichment. Sc, and to a lesser extent E, are the only ones showing a clear slope change, with S0, Sa and Sd clearly exhibiting a steady enrichment where the mass only determines the values of the metallicity, not how fast it grows.

It appears then, that the slope change that is visible for the full sample cannot be attributed solely to the mass of the galaxies. Indeed, the shape of the full sample coincides with what we would obtain by combining the earliest types (E and S0) with the latest (Sc-d) morphological types. The correlation between mass and morphology, with the later types dominating the low mass regime and the early types the high mass regime would be sufficient to explain the evolution of the MZR.

This implies that morphology is also a main actor regarding how a galaxy enriches itself. Mass determines the degree of enrichment a galaxy can achieve, and within certain morphological types it affects the speed of enrichment, but the global change in slope is mostly due to how morphology affects the ChEH.

As we progress to later types the MZR gets progressively flatter regardless of LBT, earlier types have a strong dependence on the mass but later types less so. Indeed, Sd galaxies have a flat MZR now and in the past, suggesting that they get enriched the same way irrespective of their mass.

4.2.2 Effect of star-formation stage

As we did for the evolution of the metallicity, we can separate our sample into groups depending on their star-forming status. The groups are defined as we did for the evolution of the metallicity, consistent with those identified in the star formation main sequence for galaxies.

In Fig. 9 we show the MZR for SFG, GVG, and RG galaxies.

SFG are generally less metallic than GVG and RG, and have a significantly flatter MZR, especially at recent times. SFG are also the only group to exhibit a slope change, whereas GVG and RG do not exhibit such a feature. RG do show some delay in the chemical enrichment for the lowest mass galaxies, consistent with the low mass ellipticals.

In the previous section we discussed how it appears that the slope change appears as a result of mixing galaxies of different morphology. The separation between the star-formation stages is not independent from the morphology: The RG area of the SFMS is mostly populated by early type galaxies, which on Fig. 8 all have similar shapes of the MZR. It is to be expected, then, that there is no slope change for this group. GVG are more of a mixed bag, but still much more likely to be earlier spirals than later types. The change in slope for the full population appears as a consequence of adding Sc and especially Sd galaxies. They clearly have a delayed chemical evolution for lower masses and much flatter profiles, than the earlier types. These types dominate the lower mass portion of the sample, much like the earlier types dominate the higher mass portion. It is only in the SFG group, then, that Sc-d galaxies make up a significant portion of the sample, which combined with earlier type, more massive galaxies, allows it to show the slope change in question. See Table 1 in Section 4.1.2 for the distribution of our sample in RG-GVG-SFG groups as well as the morphologies within them.

4.3 Dependence on radial distance

So far we have been analysing global properties of the galaxies over time. A detailed study of the extended properties of galaxies throughout their lifetime can be ambiguous as we would need to assume that the population of stars we analyse at each spatial position has spent the entirety of their lifetime at that same position. It has been known for some time that stellar mixing and migration affects the metallicity distribution in discs, blurring the gradients and widening the scatter in the relations (e.g. Haywood 2008; Schönrich & Binney 2009; Sánchez-Menguiano, et al. 2016; Martínez-Medina et al. 2016, 2017). Additionally, the type of analysis we are performing is blind to the effects of mergers. If a galaxy in our sample is the result of a major merger in the past what we would observe is a sort of average of the properties of the two progenitor galaxies, weighted by their relative mass. This should have little effect on the results we are reporting in regard to the global properties, as those are already the result of an combining several galaxies. For spatially resolved properties, however, mergers can affect the results as they are expected to perturb the orbits of stars significantly, driving them to a different galactocentric radius than that at which they were born.

Even with the caveats described above it is interesting to probe how the properties measured at the centre of galaxies differ from those at the outskirts. Whether this is an effect of nature (describing the original distribution of where stars were born) or modulated by migration or mergers, it is not possible to disentangle by the current observations, but can be traced by detailed simulations (e.g., Ibarra-Medel, et al. 2019).

In Fig. 10 we show the ChEHs and in Fig. 11 we show the evolution of the MZR, both measured at the centre and at two effective radii. The measurements for these quantities at the effective radius is shown in Figs. 4, 7.

In both figures we can observe that the differences between the curves get more prominent at the centre compared to those at the effective radius. Conversely, the differences get much smaller at the outskirts. This applies both to the separation in mass and time.

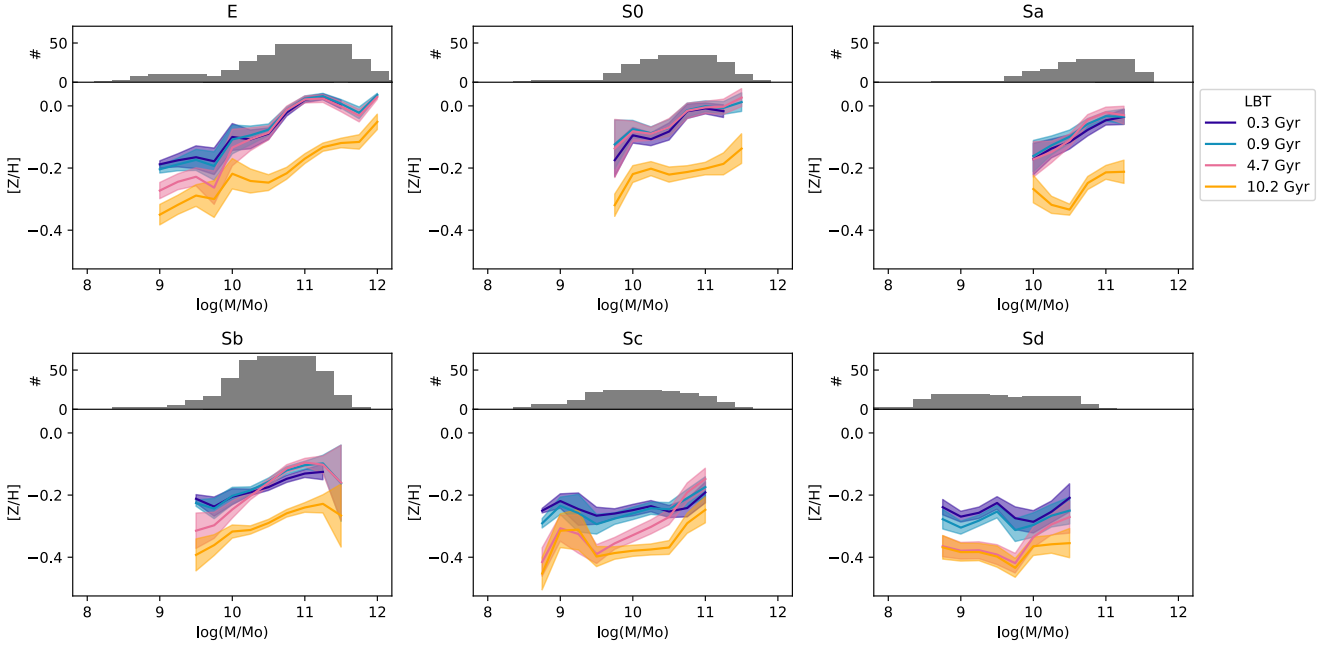


Figure 8. The bottom box of each panel shows the evolution of the MZR in time for the galaxies in our sample separated into morphological bins, with the shaded areas representing the error of the mean within that sample. On the top box of each panel a histogram showing the distribution of galaxies along the mass range is shown.

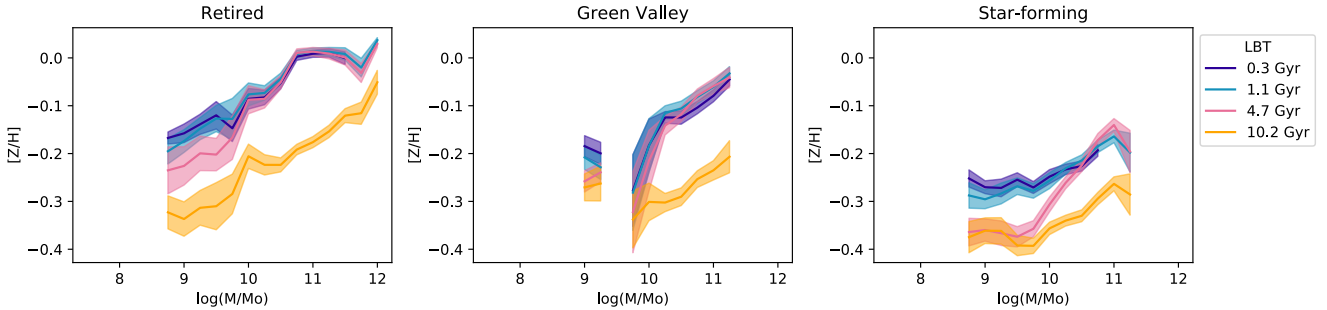


Figure 9. Evolution of the MZR in time for all the galaxies in our sample, separated by their star-forming status. On the left we show the retired galaxies, in the middle those in the Green Valley, and finally on the right the star-forming galaxies. Each line represents the MZR at a different LBT as indicated by its colour. The shaded areas represent the error of the mean ($\epsilon = \sigma/\sqrt{N}$), spanning the range between $Z/H - \epsilon_{Z/H}$ and $Z/H + \epsilon_{Z/H}$.

The ChEHs get flatter and the range between the different masses gets narrower around the ChEH for the $10^{10} - 10^{10.5}$ solar masses, which barely changes. This means that galaxies of higher masses get less metallic at the outskirts whereas galaxies less massive than this bin get more metallic compared to their centres. This shows how the less massive galaxies have a positive metallicity gradient (outside-in) and the more massive galaxies have a negative gradient (inside-out). The switch of the growth mode for low mass galaxies to outside-in has been reported in other studies (Pérez, et al. 2013; González Delgado, et al. 2017; García-Benito, et al. 2017; Goddard, et al. 2017; Sánchez 2020).

The MZR also gets flatter at the outskirts, minimising the differences between galaxies of different mass. The change in time also gets less distinct, with little evolution and no differential evolution

as a function of mass after the first growth in metallicity after the oldest MZR.

The fact that all galaxies are fairly similar at the outskirts can be understood to be the result of local downsizing (Pérez, et al. 2013; Ibarra-Medel, et al. 2016; García-Benito, et al. 2017). Galaxies roughly have exponential profiles in surface mass density, Σ_* (González Delgado, et al. 2014; Sánchez 2020). Thus a large difference in Σ_* in the centre will be much less pronounced in the outskirts. Local downsizing means that areas with similar Σ_* have evolved at a similar rate, explaining the behaviour observed here.

4.4 The variance of the shape and gap between galaxies

As described in Section 3.2 the method we employ to perform our averages within a group of galaxies allows us to separate the

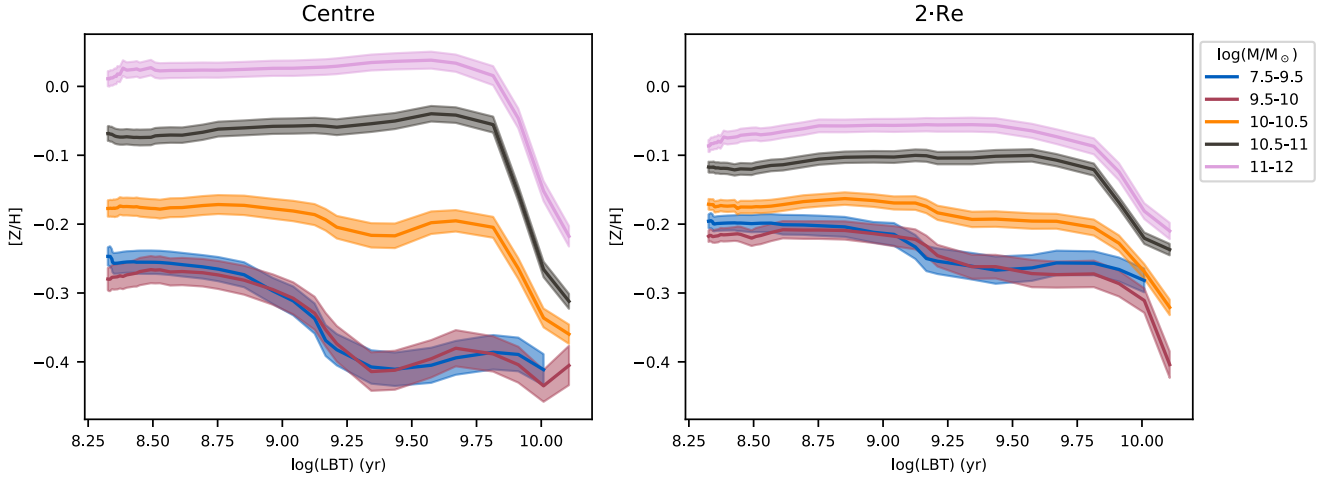


Figure 10. Evolution of the metallicity as a function of the look-back time (LBT) for all the galaxies in our sample, separated between whether the metallicity is measured at the centre or at two effective radii. Each line corresponds to a mass bin within which all the individual galaxies within the corresponding morphological bin were averaged.

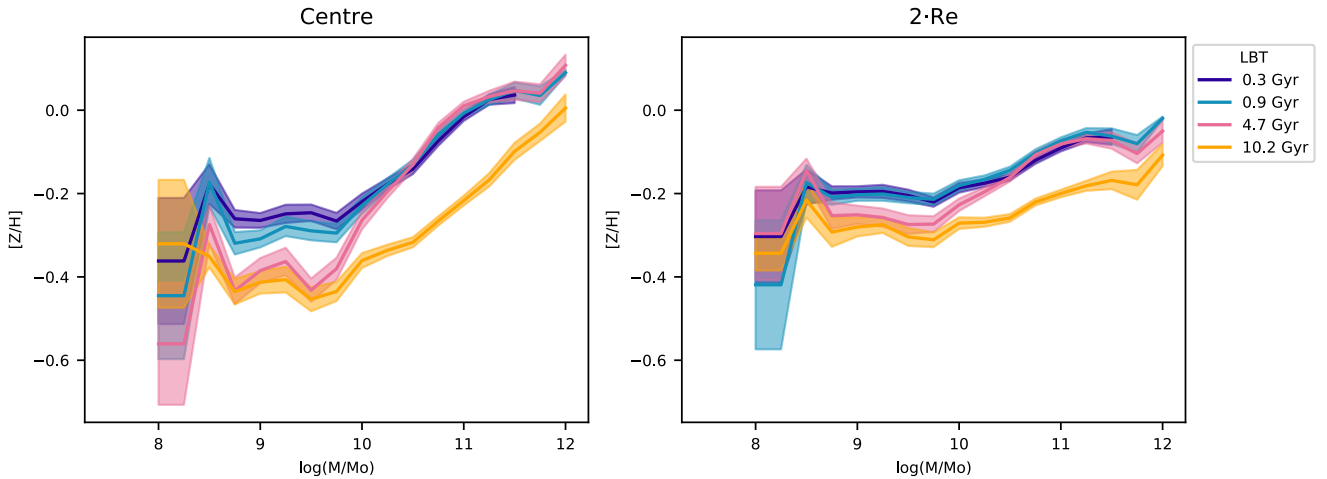


Figure 11. Evolution of the MZR in time for all the galaxies in our sample, separated between whether the metallicity is measured at the centre or at two effective radii. Each line represents the MZR at a different LBT as indicated by its colour.

variance between ChEHs into two different sources: The variance due to having a different shape and that due to a gap between curves. Two galaxies with a large shape variance but a small gap variance will have a similar value of the metallicity averaged over the LBT, but very different chemical evolution histories. On the opposite case, two galaxies with a large gap variance but a low shape variance will exhibit practically the same chemical evolution histories but with different average metallicity values over that history.

This information allows us to probe whether galaxies in a particular bin are likely to have similar chemical histories and whether they have a large variance in terms of their current metallicity.

In Figure 12 we show the values of these two variances for the mass, morphology and SFS bins used in this paper. We can observe that gap variances are generally higher than shape variances and they also have more variance within their values. They also do

not appear to exhibit any clear trends with morphology, mass or SFS.

The shape variance, on the other hand, does exhibit interesting trends. There is a trend for higher mass bins to have lower shape variance, showing that more massive galaxies have more similar ChEHs. There is also a trend with morphology, where earlier type galaxies have a lower shape variance compared to late types. When comparing between RG, GVG and SFG we see that low mass SFG have a lot more shape variance than the rest, showing also a much more pronounced separation as a result of mass than for RG and GVG.

This suggests, as it happened with the mass bins, that later type and star-forming galaxies have a higher diversity in chemical evolution histories but we need to consider one particular caveat of our analysis that could be affecting this result. Earlier type galaxies are generally "dead" galaxies whose metallicity has long stopped

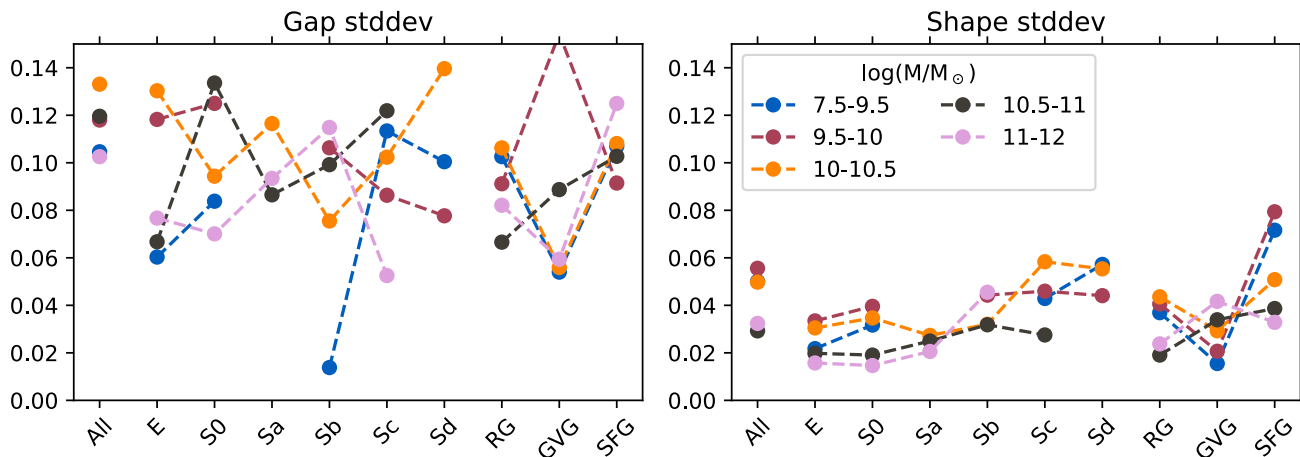


Figure 12. Gap variance (left) and shape variance (right) for galaxies in the morphology and mass bins used in this study. The gap variance is the variance between curves due only to the differences on their average values, whereas the shape variance is due to the shape of the ChEH.

evolving. The difference in the shape of their chemical evolution then, if any exists, would have happened at high LBT where our temporal resolution is much worse by construction.

It is possible, then, that the differences in morphology for the shape variance are an artefact due to the limitations of our analysis.

5 DISCUSSION

5.1 Caveats due the methodology

The results presented in this paper are strongly model-dependent. SSP fitting can yield different results depending on the fitting code, the templates used to perform the fit and the conditions that we impose such as the IMF or the dust attenuation curve (Walcher, et al. 2011; Conroy, et al. 2013; Sánchez, et al. 2016; Sánchez 2020).

In addition to these problems, there are intrinsic degeneracies in the observed spectroscopic properties among stellar populations of different physical properties. One of the most important of these degeneracies is the age-metallicity degeneracy, where a stellar template can produce a similar spectrum than one which is either younger and more metallic or older and less metallic. Despite these problems, SSP fitting codes are broadly compatible in their results, though care needs to be taken to compare them depending on their different features (Sánchez, et al. 2016).

The factor that has the most impact on the quantitative results, however, is the metallicity range that our templates have. The MILES templates are composed from observed stars. This produces more reliable templates to fit as we do not introduce a dependence on the reliability of the stellar evolution and atmosphere models, as is the case with synthetic spectra. However, they are limited to the range and sampling of physical parameters that we have available. As a result, the set of templates we have chosen from the MILES database have metallicity values no lower than $[Z/H] = -0.4$ and no higher than 0.2. While this is more than acceptable for fitting the current composition of a galaxy, we are exploring the history of metal enrichment for the galaxies in our sample. We cannot obtain values for the stellar metallicity lower than -0.4 throughout a galaxy's lifetime, which is simply not a realistic value for the early populations even if we discount the initial star formation with pristine gas.

Even so, this caveat does not completely invalidate the results we are presenting. The absolute values of the metallicity can certainly not be taken as reliable measurements at all, but the trends that they exhibit should be valid. A stellar population with $[Z/H]$ lower than -0.4 which is present within a spatial element will result in higher weights for the lower metallicity templates for that spatial element. In addition, the Age-metallicity degeneracy will most probably shift some weights towards younger stellar populations (to compensate for the lack of lower metallicity populations). This may affect the SFH more than the ChEH. However, as demonstrated by Ibarra-Medel, et al. (2019), based on hydrodynamic simulations, the effect is not dramatically strong.

The sampling in the temporal dimension covers a wide range of ages, but it is uneven, with much shorter intervals for recent ages. This is by construction. This sampling was adopted since our ability to distinguish between different stellar populations is less precise for older than for younger stellar populations. Thus, stellar populations differentiate themselves following an almost logarithmic sampling. In other words, two stellar populations of an age of hundred of Myrs differentiate themselves well when they have a difference in age of ~ 100 Myr. For stellar populations of few Gyrs, they present different spectra when they have differences in age of more than ~ 1 Gyr.

In conclusion, the degeneracies and uncertainties in the method employed here mean that we cannot take quantitative measurements at face value and individual features of a single galaxy's ChEH or MZR (t) curve can easily be artefacts. However, the qualitative behaviour of the averaged curves and their features which are consistent between mass and morphology bins should not arise from artefacts related to the fitting method employed. This is a similar conclusion to that of Ibarra-Medel, et al. (2019), based on simulations. It would certainly be of interest, however, to repeat this study using a different set of SSP and/or a different galaxy sample such as MaNGA, SAMI or AMUSING++ as future work on this topic. We will perform this exploration in further studies.

5.2 Previous explorations of MZR(t)

Existing studies on how the stellar MZR changes through time are Panter, et al. (2008) and Vale Asari, et al. (2009), for a similar analysis to ours, and VANDELS (Cullen, et al. 2019), which fit stellar templates to galaxies observed at high redshift. Our results are broadly compatible with these studies from a qualitative point of view.

All studies, including the current one, agree on that at high redshifts the MZR was steeper than now. They agree too in that massive galaxies were enriched faster than lower-mass ones. However, Vale Asari, et al. (2009) does not see the flattening of the MZR for low-mass galaxies. This is expected as their sample only includes galaxies down to $10^{10} M_{\odot}$. This is well above the value at which the MZR appears to flatten in our results. On the other hand, VANDELS does appear to show some flattening at low masses, starting from around $10^{9.5}$ to $10^{10} M_{\odot}$. This is consistent with our results.

There are large discrepancies as to the quantitative values, with our results having a narrower range of metallicities and especially our metallicity values for high redshifts are much higher, not going below -0.4 as compared to VANDELS or Vale Asari, et al. (2009) which reach values of -1.0 for high redshifts. This discrepancy is expected as a result of the choice in stellar templates as described above, as our SSP are composed from observed stars which limits our range of metallicities to between -0.4 and 0.2. All the above mentioned studies use synthetic templates which provide as wide a range of physical parameters in exchange for a dependence on theoretical models.

5.3 [Z/H] (t) convergence in SFGs along the last few Gyr

One of the most interesting results we report in this study refers to the metallicity evolution for star-forming galaxies compared to those that are retired or populate the green valley. These show a convergence in their values at recent times, with the more massive galaxies reaching a maximum early and the less massive ones only just getting enriched to that value. GVG and RG, on the other hand, show a more stratified evolution, especially the retired galaxies. What makes this result particularly relevant is the fact that this behaviour is only observed when we separate galaxies by star-forming status.

It is well-known that morphology and star formation status are not independent from each other. Late galaxy types are preferentially populating the SF sequence of the SFMS and earlier types appearing mostly at the GV and RG areas instead. However, the two most massive bins of galaxies in our study are not populated by Sd, with the most massive bin only being populated by Sa and Sb. By comparing Figs. 5 and 6 we can see that there is a marked difference in the metallicity value for the most massive bin of SFG and the values for Sa-b galaxies. Since all SFG of that mass are in the aforementioned mass-morphology bins it means that the difference, which produces the convergence of values with the less massive bins, is due only to their star-forming status.

Another effect that is observed is a slight, steady, decrease in metallicity for the more massive bins after the initial enrichment. This effect can be seen clearly for SFG and for the $10^{10.5-11} M_{\odot}$ bin for GVG. The GVG galaxies for three bins also appear to show some convergence to a lesser extent than SFG. Given that GVG are generally considered to be transitioning from SFG to RG we can consider this behaviour to be tied to that of the SFG.

The convergence observed suggests that there is some regu-

latory mechanism that limits how high a metallicity a star-forming galaxy can achieve. Looking at the Sc galaxies in Fig. 5 we might be tempted to claim that the convergence effect is nothing more than the result of mixing morphologies, as the more massive galaxies have a flatter evolution and the less massive galaxies are still growing, but this interpretation does not explain the convergence nor why the massive Sa-b galaxies drop about 0.1-0.2 dex in metallicity when considering only the star-forming galaxies, a drop that produces the observed convergence. It is more likely, then, that Sc show the same behaviour because they are dominated by SFG.

It has been shown that stellar feedback in the form of metal-rich outflows remove metals from galaxies which can result in a regulatory process where the metals can achieve an equilibrium between production and removal. This has been proposed as a mechanism that explains or contributes to the flattening of the nebular MZR at high galaxy masses (Tremonti, et al. 2004; Mannucci, et al. 2010; Sánchez, et al. 2013; Belfiore, et al. 2017; Barrera-Ballesteros, et al. 2018). While this mechanism undoubtedly contributes to the convergence it is not enough by itself. The reason for this is the differences between SFG-GVG-RG, with the SFG collapsing to a value of metallicity much lower than for GVG and especially RG. In order to produce the observed results a mechanism unique to galaxies with a sustained star-formation is required. The two most massive bins of RG clearly collapse to a maximum value, an effect that can be attributed to the regulation via only outflows and quenching.

As for the additional mechanism for SFG, we believe the easiest answer would be inflows of pristine gas which sustains star-formation. This mechanism has long been proposed to explain how many galaxies appear to maintain a steady star formation rate over time periods much longer than the time it would take to exhaust the available gas within them as well as to reduce the metallicity reached by the formed stars. These observations have motivated the development of chemical evolution models generally referred to as ‘gas regulatory’ or ‘bathtub’ models (Finlator & Davé 2008; Lilly, et al. 2013; Dekel, et al. 2013; Peng & Maiolino 2014; Barrera-Ballesteros, et al. 2018; Belfiore, et al. 2019) Within these models there is a sustained inflow of pristine gas from the halo into the galaxy which provides the material required to maintain star formation over long times, as well as outflows which regulate the gas content.

This scenario does conform to what we observe in our results. As the original gas in the disc is used up to form stars it gets progressively more metallic from the previously formed stars polluting their environment. Once the original gas starts to be exhausted the inflow mechanisms start to become more relevant to sustain further star-formation and newer stars no longer necessarily have higher metallicities than the current population. This can produce the observed convergence, as well as the subtler steady decrease in metallicity after the initial enrichment.

The fact that the decrease is only observed for the more massive bins is counter-intuitive as more massive galaxies have more massive haloes. Thus, these mechanisms should be less effective. One possible explanation is that the less massive galaxies have a higher fraction of the primordial gas in their disk. As a result, inflow-sustained star formation does not diminish the metallicity because these galaxies have not yet reached their maximum values as a result of their delayed evolution. In this manner, even though they also have inflows, this does not produce the decrease in metallicity that is observed for the more massive galaxies which exhausted their primordial gas reserve long ago.

Another explanation is that the observed effect is a result of

high mass SFG being a peculiar sample. Downsizing predicts that the more massive galaxies should form stars faster, which combined with less efficient gas inflows means that they should exhaust their gas very quickly. In order for a galaxy to maintain a high SFR while being in the most massive bin it would require an unusually massive inflow sustained through its lifetime. In this scenario, the "normal" galaxies do not populate this particular group at all, leaving only the outliers. The behaviour of these galaxies would therefore not be representative of galaxies in general, avoiding the discrepancy.

A potential caveat to this interpretation, which in turn affects all results derived from the SFS-GV-R separation, is that we are analysing the history of a galaxy based on current and transient properties. We evaluate as star-forming those galaxies that have a high value of $EW_{H\alpha}$ (above 6 Å), but the equivalent width traces only ongoing star formation. However, recent results have shown that indeed most current SFGs have been SF along their life time (e.g. Pandya, et al. 2017; Sánchez, et al. 2019 and references therein). This ensures that the results we present obtained by tracing the evolution of a group of currently star-forming galaxies are valid, as statistically most of these galaxies have belonged to this group throughout their history.

5.4 Caveats and effects of the morphology

A similar caveat to the segregation by the star-forming status can be found for the separation by morphology. The morphology classification is determined based on the current appearance that the galaxies in our sample exhibit. However, fossil record techniques do not provide information to infer the morphology of a galaxy in the past at least with the spatial resolution and bin performed to recover the resolved SFH. Fossil record data obtained from high resolution IFS observations such as MUSE might be able to achieve this, though it would still be limited by the effect that radial migrations could have on the distribution of stars.

Understanding the morphological evolution of galaxies is an ongoing effort in the field. Conselice (2014) reviews the topic, including surveys of multi-redshift observations using deep-field imaging to determine the morphologies of galaxies in the past, such as CANDELS (Grogin, et al. 2011; Koekemoer, et al. 2011). The main results are that the current Hubble type classification stops being representative of galaxies at around redshift 2, with the number of peculiar galaxies growing until it dominates the population. As we move towards closer times the fraction of peculiar galaxies drops drastically while that of disk galaxies and especially spheroidals grow. This means that morphology evolution is not simply a process of galaxies "switching" between the morphological types we currently observe, but an evolution towards them. When we show the evolution of the metallicity or the MZR within a morphological bin, then, it should be understood as the evolution of galaxies whose shape ends up as that morphological type.

As discussed before most of the qualitative results regarding the evolution of the MZR(t), involving a change in its slope and the subsequent flattening in recent times at high mass values, was already found in the literature (Panter, et al. 2008; Vale Asari, et al. 2009; Cullen, et al. 2019). This flattening represents the well-established idea that more massive galaxies evolve faster and low mass galaxies have a slower evolution. This is related to the phenomenon of downsizing, where mass (or Σ_{star} for local downsizing) correlates negatively with star formation rate. This means that more massive galaxies have lower SFR (in the nearby Universe), and in the local version, the areas of a galaxy with higher Σ_{star} have lower surface SFR density (e.g. Cano-Díaz, et al. 2019). This result

highlights the apparent importance of the M_{star} in the shaping the chemical evolution of galaxies.

As indicated in Sec. 4.2, we reproduce the change in slope for the MZR when considering the entire sample (apart from an initial increase in slope after the furthest age). But this feature does not appear as clearly when we separate the galaxies into different morphology bins (Fig. 8, Sec. 4.2.1). This suggests that it is not only mass that regulates how fast a galaxy gets enriched, but also the morphology plays an important role. In fact, combining the MZR for the early type galaxies in the high mass regime with the MZR for the late type galaxies in the low mass regime we recover the general apparent trend.

There are two morphological bins that exhibit a slope change: Sc and E. This can also be inferred from the ChEH for these galaxies. There is a marked change in the ChEH for Sc between the most massive bin and the rest, with the former showing a fast initial enrichment similar to the Sa-b bins whereas the latter, low-mass bins, are similar to the ChEHs of Sd galaxies. For E galaxies, it appears that the low mass portion has a different, delayed evolution with a still growing metallicity.

5.5 Effects of radial variation of [Z/H]

The metallicity values presented here are measured at the effective radius of each galaxy. Measuring physical parameters at the effective radius is a good proxy for their global value in a galaxy (Sánchez 2020). Defining the effective radius as the distance at which to make the measurements is also a good way to compare galaxies of different sizes in a consistent manner.

One might expect that measuring [Z/H] at the centre instead would provide a more reliable estimation, due to the systematic higher S/N. However the centres of galaxies are not necessarily good proxies for their global properties. Furthermore, the centre of galaxies could present physical phenomena (like AGNs) that may affect the current estimations.

We presented in Figs. 10-11 the evolution of the metallicity and MZR at different galactocentric distances. These are not direct measurements such as for Re but inferences using the slope of the metallicity gradient (at each look-back time). It is clear that at the outskirts the M_{star} of galaxies is less relevant as proxies of the metallicities than at one effective radius and even more so at the centre, where the opposite trend is observed (i.e., a stronger dependency with the M_{star}). The immediate conclusion, then, is that the chemical enrichment in the outskirts is relatively similar for different galaxies when compared to the global evolution and especially to the centres. This is consistent with the effect of the local downsizing. However, it could also be a consequence of the difference between the radial profiles of low mass galaxies (rising from the inside-out) and those of more massive ones (declining from the inside-out). It is readily apparent in Fig. 10 that the more massive bins have higher metallicities at the centre than at the outskirts, whereas for low mass galaxies the metallicity at the outskirts is higher than at the centre.

It bears mention that the gradient adopted to derive the inner- and outer-most metallicities is assumed to be linear (following Sánchez, et al. 2018), so any deviations from this behaviour will introduce uncertainties in the values. This, however, is not expected to be a significant effect when averaging over several galaxies, and certainly should not affect the qualitative behaviours we are reporting here.

5.6 Effects of stellar migration and mixing

Fossil record techniques allow us to reliably obtain either the global history or the current resolved properties of a galaxy. The spatially resolved history, however, has an intrinsic caveat in that we are observing the stellar populations at their current position. Any temporal changes to the spatial structure of the galaxy or stellar migrations are lost when using this technique. The degree to which stars mix and migrate through a galaxy is an ongoing topic in extra-galactic studies (e.g. Haywood 2008; Schönrich & Binney 2009; Minchev & Famaey 2010; Di Matteo, et al. 2013; Sánchez-Menguiano, et al. 2016, 2018)

Fortunately, we do not expect these effects to produce spurious results but rather to prevent actual features from being observed. This is because the migration of stars does not have an intrinsic dependence on their physical parameters such as the metallicity. There is, however, a dependence on the age because the older stars have had more time to be affected by these processes. Still, any differences that we observe today as a factor of spatial position should be real, if more difficult to determine as a result of the mixing of stars and not reliable from a quantitative point of view. Most of the current simulations of radial migration describe a general increase in the dispersion of the radial distributions rather than a global change in their profiles (Minchev & Famaey 2010; Di Matteo, et al. 2013). In general, radial trends are slightly smoother and their signature mitigated or even blurred (in the extreme cases). Thus, any radial difference observed in the average properties using the fossil record could be considered as a lower limit to the one that would be observed without migration/mixing.

5.7 The $Z(t)$ gap for different masses and morphologies

The ChEHs for spiral galaxies exhibit an interesting feature: for those late type galaxies that populate all mass bins, the gaps between the curves for different masses get progressively narrower from Sa to Sc. This appears to imply that for spirals the later the morphological type the less difference in metallicity between galaxies as a result of their differing masses. This effect can also be observed in the MZR(t) as a progressive flattening towards later types. In fact, using the MZR(t), the result holds even considering the Sd galaxies, which exhibit a practically flat relation.

This feature provides further support for the notion discussed before that it is morphology, and not mass, that is the main driver of the shape of the ChEH.

For very late type galaxies (Sd bin) M_* appears to be largely irrelevant to the enrichment process. Do note, however, that this is not necessarily valid for dwarf galaxies which lie much below our mass range (in general). It would certainly be of interest, however, to repeat this study for a comprehensive sample of dwarf galaxies to answer the following questions: Are dwarf galaxies their own group in terms of chemical enrichment or do they exhibit morphology dependence as the ones in our sample? Do dwarf galaxies of a morphological type (for example, dwarf ellipticals) appear as an extension of the relation for their type?. Unfortunately our sample does not cover the required mass range to address these questions.

5.8 Relations between the ChEH and the SFR'

The derivative of the mass (SFR') is somewhat equivalent to the SFH of a galaxy, as rapid changes in the mass of a galaxy are necessarily associated to episodes of star formation. The difference is that while the SFH only traces the addition of new stars the SFR'

also includes the death of preexisting stars. The latter phenomenon, however, manifests as a steady decrease in M_* as the lifetimes of stars depend on their mass. Because of this if a peak appears on the SFR' it represents a burst of star formation.

The peaks in SFR' that we observe appear to be associated with either a dip or a jump between two somewhat flat regimes of the metallicity growth. Both regimes should represent episodes of intense star formation among all galaxies in the considered mass-morphology bin. All galaxies may have individual bursts of star formation throughout their life-times. However, this appears to be a global burst of star-formation which stands out even after averaging different galaxies with different histories. The same conclusion can be reached for the dip or flattening: for such a feature to consistently appear when we average over several galaxies indicates that the phenomenon is global. This does not mean that all galaxies should exhibit these two features individually. For the effect to arise on the average it would be enough if it was more likely for galaxies to have a burst of star formation and a decrease in metallicity at these times than others.

The physical link between the two is also not clear. We have two possible interpretations: (i) a dip in the metallicity in a otherwise steadily growing curve and (ii) a sharp increase in metallicity which connects two comparatively flat regimes. The first scenario implies that a new generation of stars which is very poor in metals was produced. This is the only way to produce a decrease of metallicity in the global trend. For the second scenario it means stars are generally produced with a very slow growth in metallicity over time except for a sharp increase which appears immediately after the burst, suggesting an input generation of stars of very high metallicity. The following generations of stars, on the other hand, should not be as high in metallicity as the growth curve would not be as flat as it appears otherwise.

This phenomenon correlates with the morphological type and especially the mass of the galaxies. It is more prominent for later and less massive galaxies. Indeed, the more massive bins do not exhibit a visible dip in metallicity except for Sc galaxies. The higher prominence for late type and low-mass galaxies suggests that this may be related to the gas content of galaxies, as both of these properties correlate with higher gas content. Even if this is the case, however, there is no clear link between a galaxy having a high gas content and it suffering an episode of star formation. This is especially so for a galaxy with a stellar metallicity which greatly differs from the value that would be expected from its previous evolution. A massive inflow of pristine, or very poor metal gas could cause an important SFR burst and, consequently, a fast (\sim Myr) increase of the metallicity of the ISM. Therefore, most stars formed during the burst could present high metallicity. If the metallicity of the ISM before the burst is low (as is the case of low-mass galaxies), the metallicity increase is higher. Moreover, if well-mixed outflows occur during the burst, the metallicity increase is even higher.

6 SUMMARY AND CONCLUSIONS

- We have used fossil record techniques to study the chemical evolution of a sample of galaxies observed with IFS (CALIFA). The analysis allows us to measure the stellar metallicity at different cosmological times.

- The chemical enrichment history of galaxies shows a faster evolution for the more massive and earlier type galaxies, which also have higher terminal values of the metallicity. The lower mass and latter type galaxies have lower metallicities and appear to still

be steadily increasing their metallicity, a sign that they are still assembling their mass.

- Star-forming galaxies appear to have an upper limit of metallicity towards which they converge, regardless of stellar mass. The most massive bins show a noticeable decrease in metallicity for SFG, as well as for GVG to a lesser degree.

- The MZR shows a slope change resulting from the more massive galaxies evolving faster than the less massive ones. Upon separating the galaxies into morphology bins, however, this behaviour becomes much less pronounced, suggesting that morphology is an important factor in determining how fast galaxies evolve.

- Galaxies evolve more similarly in the outskirts compared to the centre or the effective radius, with low mass galaxies showing a positive metallicity gradient.

- The chemical enrichment histories of galaxies differ more in terms of absolute value rather than on their shapes. While their differences due to their absolute values have no correlation to mass, morphology, or star-forming status there is a clear correlation regarding their difference in shape. Earlier, more massive and retired galaxies have more similar evolutions, while later, less massive and star-forming galaxies have more differences between the shape of their enrichment curves.

ACKNOWLEDGEMENTS

We are grateful for the support of a CONACYT grant CB-285080 and FC-2016-01-1916, and funding from the PAPIIT-DGAPA-IN100519 (UNAM) project. L.G. was funded by the European Union's Horizon 2020 research and innovation programme under the Marie Skłodowska-Curie grant agreement No. 839090. This work has been partially supported by the Spanish grant PGC2018-095317-B-C21 within the European Funds for Regional Development (FEDER).

DATA AVAILABILITY

The data used in this article consists of the publicly available DR3 of the CALIFA survey as well as extended surveys such as PISCO. CALIFA DR3 data cubes can be accessed at https://califaserv.caha.es/CALIFA_WEB/public_html/?q=content/califa-3rd-data-release, with direct access to the V500 version used in this article available at ftp://ftp.caha.es/CALIFA/reduced/V500/reduced_v2.2/.

The extended survey data can be shared on reasonable request by contacting SFS and LG.

REFERENCES

Abazajian K. N., et al., 2009, *ApJS*, 182, 543
 Barrera-Ballesteros J. K., Sánchez S. F., Heckman T., Blanc G. A., MaNGA Team, 2017, *ApJ*, 844, 80
 Barrera-Ballesteros J. K., et al., 2018, *ApJ*, 852, 74
 Bitsakis T., et al., 2018, *ApJ*, 853, 104
 Belfiore F., Maiolino R., Bothwell M., 2016, *MNRAS*, 455, 1218
 Belfiore F., Vincenzo F., Maiolino R., Matteucci F., 2019, *MNRAS*, 487, 456
 Belfiore F., et al., 2017, *MNRAS*, 469, 151
 Blanton M. R., Moustakas J., 2009, *ARA&A*, 47, 159
 Bundy K., et al., 2015, *ApJ*, 798, 7

Cano-Díaz M., Ávila-Reese V., Sánchez S. F., Hernández-Toledo H. M., Rodríguez-Puebla A., Boquien M., Ibarra-Medel H., 2019, *MNRAS*, 488, 3929
 Cano-Díaz M., et al., 2016, *ApJL*, 821, L26
 Cid Fernandes R., et al., 2013, *A&A*, 557, A86
 Combes F., 2014, *ASPC*, 480, 211, *ASPC*.480
 Conroy C., Dutton A. A., Graves G. J., Mendel J. T., van Dokkum P. G., 2013, *ApJL*, 776, L26
 Conselice C. J., 2014, *ARA&A*, 52, 291
 Cullen F., et al., 2019, *MNRAS*, 487, 2038
 Davé R., Finlator K., Oppenheimer B. D., 2011, *MNRAS*, 416, 1354
 Dekel A., Zolotov A., Tweed D., Cacciato M., Ceverino D., Primack J. R., 2013, *MNRAS*, 435, 999
 Dekel A., Krumholz M. R., 2013, *MNRAS*, 432, 455
 Di Matteo P., Haywood M., Combes F., Semelin B., Snaith O. N., 2013, *A&A*, 553, A102
 Erroz-Ferrer S., et al., 2019, *MNRAS*, 484, 5009
 Espinosa-Ponce C., et al., 2020, *MNRAS*, 494, 1622
 Finlator K., Davé R., 2008, *MNRAS*, 385, 2181
 Galbany L., Anderson J. P., Sánchez S. F., Kuncarayakti H., Pedraz S., González-Gaitán S., Stanishv V., et al., 2018, *ApJ*, 855, 107
 Gallazzi A., Charlot S., Brinchmann J., White S. D. M., Tremonti C. A., 2005, *MNRAS*, 362, 41
 García-Benito R., et al., 2015, *A&A*, 576, A135
 García-Benito R., et al., 2017, *A&A*, 608, A27
 Goddard D., et al., 2017, *MNRAS*, 466, 4731
 González Delgado R. M., Cerviño M., Martins L. P., Leitherer C., Hauschildt P. H., 2005, *MNRAS*, 357, 945
 González Delgado R. M., et al., 2014, *A&A*, 562, A47
 González Delgado R. M., et al., 2014, *ApJL*, 791, L16
 González Delgado R. M., et al., 2015, *A&A*, 581, A103
 González Delgado R. M., et al., 2017, *A&A*, 607, A128
 Grogin N. A., et al., 2011, *ApJS*, 197, 35
 Haywood M., 2008, *MNRAS*, 388, 1175
 Husemann B., et al., 2013, *A&A*, 549, A87
 Ibarra-Medel H. J., et al., 2016, *MNRAS*, 463, 2799
 Ibarra-Medel H. J., Ávila-Reese V., Sánchez S. F., González-Samaniego A., Rodríguez-Puebla A., 2019, *MNRAS*, 483, 4525
 Kauffmann G., et al., 2003, *MNRAS*, 341, 33
 Kashino D., et al., 2017, *ApJ*, 835, 88
 Kelz A., et al., 2006, *PASP*, 118, 129
 Kewley L. J., Ellison S. L., 2008, *ApJ*, 681, 1183
 Koekemoer A. M., et al., 2011, *ApJS*, 197, 36
 Lacerda E. A. D., Sánchez S. F., Cid Fernandes R., López-Cobá C., Espinosa-Ponce C., Galbany L., 2020, *MNRAS*, 492, 3073
 Lara-López M. A., et al., 2013, *MNRAS*, 434, 451
 Lequeux J., Peimbert M., Rayo J. F., Serrano A., Torres-Peimbert S., 1979, *A&A*, 500, 145
 Lian J., Thomas D., Maraston C., 2018, *MNRAS*, 481, 4000
 Lilly S. J., Carollo C. M., Pipino A., Renzini A., Peng Y., 2013, *ApJ*, 772, 119
 López Fernández R., González Delgado R. M., Pérez E., García-Benito R., Cid Fernandes R., Schoenell W., Sánchez S. F., et al., 2018, *A&A*, 615, A27
 Mannucci F., Cresci G., Maiolino R., Marconi A., Gnerucci A., 2010, *MNRAS*, 408, 2115
 Martínez-Medina L. A., Pichardo B., Moreno E., Peimbert A., 2016, *MNRAS*, 463, 459
 Martínez-Medina L. A., Pichardo B., Peimbert A., Carigi L., 2017, *MNRAS*, 468, 3615
 McQuinn K. B. W., et al., 2010, *ApJ*, 724, 49
 Minchev I., Famaey B., 2010, *ApJ*, 722, 112
 Moran S. M., et al., 2012, *ApJ*, 745, 66
 Muzzin A., et al., 2013, *ApJ*, 777, 18
 Onodera M., et al., 2015, *ApJ*, 808, 161
 Pandya V., et al., 2017, *MNRAS*, 472, 2054
 Panter B., Jimenez R., Heavens A. F., Charlot S., 2007, *MNRAS*, 378, 1550
 Panter B., Jimenez R., Heavens A. F., Charlot S., 2008, *MNRAS*, 391, 1117

- Peng Y.-jie., Maiolino R., 2014, MNRAS, 443, 3643
 Pérez-González P. G., et al., 2008, ApJ, 675, 234
 Pérez E., et al., 2013, ApJL, 764, L1
 Rodríguez-Puebla A., Primack J. R., Avila-Reese V., Faber S. M., 2017, MNRAS, 470, 651
 Rosales-Ortega F. F., et al., 2012, ApJL, 756, L31
 Edwin E. Salpeter, 1955, ApJ, 121, 161
 Sancisi R., Fraternali F., Oosterloo T., van der Hulst T., 2008, A&ARv, 15, 189
 Sanders R. L., et al., 2015, ApJ, 799, 138
 Schönrich R., Binney J., 2009, MNRAS, 396, 203
 Steidel C. C., et al., 2014, ApJ, 795, 165
 Sánchez-Blázquez P., Ocavirk P., Gibson B. K., Pérez I., Peletier R. F., 2011, MNRAS, 415, 709
 Sánchez-Menguiano L., et al., 2018, A&A, 609, A119
 Sánchez-Menguiano L., et al., 2016, ApJL, 830, L40
 Sánchez S. F., 2006, AN, 327, 850
 Sánchez S. F., Cardiel N., Verheijen M. A. W., Pedraz S., Covone G., 2007, MNRAS, 376, 125
 Sánchez S. F., et al., 2016, A&A, 594, A36
 Sánchez S. F., et al., 2018, RMxAA, 54, 217
 Sánchez S. F., et al., 2013, A&A, 554, A58
 Sánchez S. F., et al., 2019, MNRAS, 482, 1557
 Sánchez S. F., et al., 2019, MNRAS, 484, 3042
 Sánchez S. F., et al., 2012, A&A, 538, A8
 Sánchez S. F., et al., 2016, RMxAA, 52, 21
 Sánchez S. F., et al., 2016, RMxAA, 52, 171
 Sánchez S. F., et al., 2017, MNRAS, 469, 2121
 Sánchez S. F., 2020, ARA&A, 58, annurev
 Thomas D., Maraston C., Bender R., Mendes de Oliveira C., 2005, ApJ, 621, 673
 Thomas D., Maraston C., Schawinski K., Sarzi M., Silk J., 2010, MNRAS, 404, 1775
 Tremonti C. A., et al., 2004, ApJ, 613, 898
 Troncoso P., et al., 2014, A&A, 563, A58
 Vale Asari N., Stasińska G., Cid Fernandes R., Gomes J. M., Schlickmann M., Mateus A., Schoenell W., 2009, MNRAS, 396, L71
 Vazdekis A., Peletier R. F., Beckman J. E., Casuso E., 1997, ApJS, 111, 203
 Vazdekis A., Sánchez-Blázquez P., Falcón-Barroso J., Cenarro A. J., Beasley M. A., Cardiel N., Gorgas J., et al., 2010, MNRAS, 404, 1639
 Wake D. A., et al., 2017, AJ, 154, 86
 Walcher C. J., et al., 2014, A&A, 569, A1
 Walcher J., Groves B., Budavári T., Dale D., 2011, Ap&SS, 331, 1
 Worthey G., 1994, ApJS, 95, 107
 Wuyts E., et al., 2014, ApJL, 789, L40
 Young J. S., Allen L., Kenney J. D. P., Lesser A., Rownd B., 1996, AJ, 112, 1903
 Zahid H. J., et al., 2014, ApJ, 791, 130